Observation of Reentrant Correlated Insulators and Interaction-Driven Fermi-Surface Reconstructions at One Magnetic Flux Quantum per Moiré Unit Cell in Magic-Angle Twisted Bilayer Graphene

Ipsita Das,[1] Cheng Shen,[1] Alexandre Jaoui,[1] Jonah Herzog-Arbeitman,[2] Aaron Chew,[2] Chang-Woo Cho,[3] Kenji Watanabe,[4] Takashi Taniguchi,[5] Benjamin A. Piot,[3] B. Andrei Bernevig,[2] and Dmitri K. Efetov[1,*]

[1]*ICFO—Institut de Ciencies Fotoniques, The Barcelona Institute of Science and Technology, Castelldefels, Barcelona 08860, Spain*

[2]*Department of Physics, Princeton University, Princeton, New Jersey 08544, USA*

[3]*Laboratoire National des Champs Magnétiques Intenses, Université Grenoble Alpes, UPS-INSA-EMFL-CNRS-LNCMI, 25 avenue des Martyrs, 38042 Grenoble, France*

[4]*Research Center for Functional Materials, National Institute for Materials Science, 1-1 Namiki, Tsukuba 305-0044, Japan*

[5]*International Center for Materials Nanoarchitectonics, National Institute for Materials Science, 1-1 Namiki, Tsukuba 305-0044, Japan*

(Received 22 November 2021; accepted 30 March 2022; published 23 May 2022)

The discovery of flat bands with nontrivial band topology in magic-angle twisted bilayer graphene (MATBG) has provided a unique platform to study strongly correlated phenomena including superconductivity, correlated insulators, Chern insulators, and magnetism. A fundamental feature of the MATBG, so far unexplored, is its high magnetic field Hofstadter spectrum. Here, we report on a detailed magnetotransport study of a MATBG device in external magnetic fields of up to $B = 31$ T, corresponding to one magnetic flux quantum per moiré unit cell Φ_0. At Φ_0, we observe reentrant correlated insulators at a flat band filling factors of $\nu = +2$ and of $\nu = +3$, and interaction-driven Fermi-surface reconstructions at other fillings, which are identified by new sets of Landau levels originating from these. These experimental observations are supplemented by theoretical work that predicts a new set of eight well-isolated flat bands at Φ_0, of comparable band width, but with different topology than in zero field. Overall, our magnetotransport data reveal a qualitatively new Hofstadter spectrum in MATBG, which arises due to the strong electronic correlations in the reentrant flat bands.

DOI: 10.1103/PhysRevLett.128.217701

Two superimposed graphene monolayers, misaligned by a small twist angle $\theta = 1.1°$, produce eight electronic flat bands near the charge neutrality point (CNP) [1]. These bands host strong electronic interactions and provide an exciting platform to study exotic quantum phenomena, such as correlated insulators [2–5], superconductors [3,4,6–8], magnets [3,9–11], strange metals [12,13], etc. The moiré superpotential in magic-angle twisted bilayer graphene (MATBG) creates a new set of renormalized bands in a mini-Brillouin zone, which possess C_{2z}, C_{3z}, and C_{2x} rotational symmetries and time reversal symmetry T at zero magnetic field. Nonzero Dirac helicity in MATBG, protected by the $C_{2z}T$ symmetry and the decoupled valleys, gives rise to the nontrivial band topology [14–16]. As the role of the symmetries in the observed quantum phases in MATBG is still a topic of active investigation, discovering novel flat band systems with different inherent symmetries, but similar phenomenology, is a major goal in the field.

Our exact theoretical study of the Bistritzer-MacDonald (BM) Hofstadter spectrum has uncovered a set of low-energy flat bands at one quantum of magnetic flux per moiré unit cell Φ_0 [17]. While strong magnetic fields tend to break the bands into fractal Hofstadter subbands, here due to the Aharonov-Bohm effect, full density Bloch-like bands reemerge at Φ_0. The moiré unit cell area of MATBG is almost 3000 times larger than the graphene unit cell; thus, the magnetic field required to reach one full flux quantum is far smaller, close to 30 T, and is within experimental reach [18,19]. Although previous studies of the electronic properties of graphene–hexagonal boron nitride (h-BN) superlattice in the presence of high magnetic fields have provided great insight into the Hofstadter spectrum [20–27], flat electronic bands with strong correlations have never been explored in this light before. Together, these characteristics make MATBG an unprecedented platform to study the Hofstadter spectrum enriched by band topology and strong interactions.

Here, we report on the detailed magnetotransport behavior of a MATBG device with a twist angle $\theta = 1.12° \pm 0.02°$ in the presence of an external perpendicular magnetic field as high as 31 T. We resolve the continuous evolution of the Hofstadter spectrum from zero field to Φ_0, which corresponds to a B field of $B_0 = 30.5$ T. At B_0 we observe reentrant correlated insulators at certain integer

 © 2022 American Physical Society

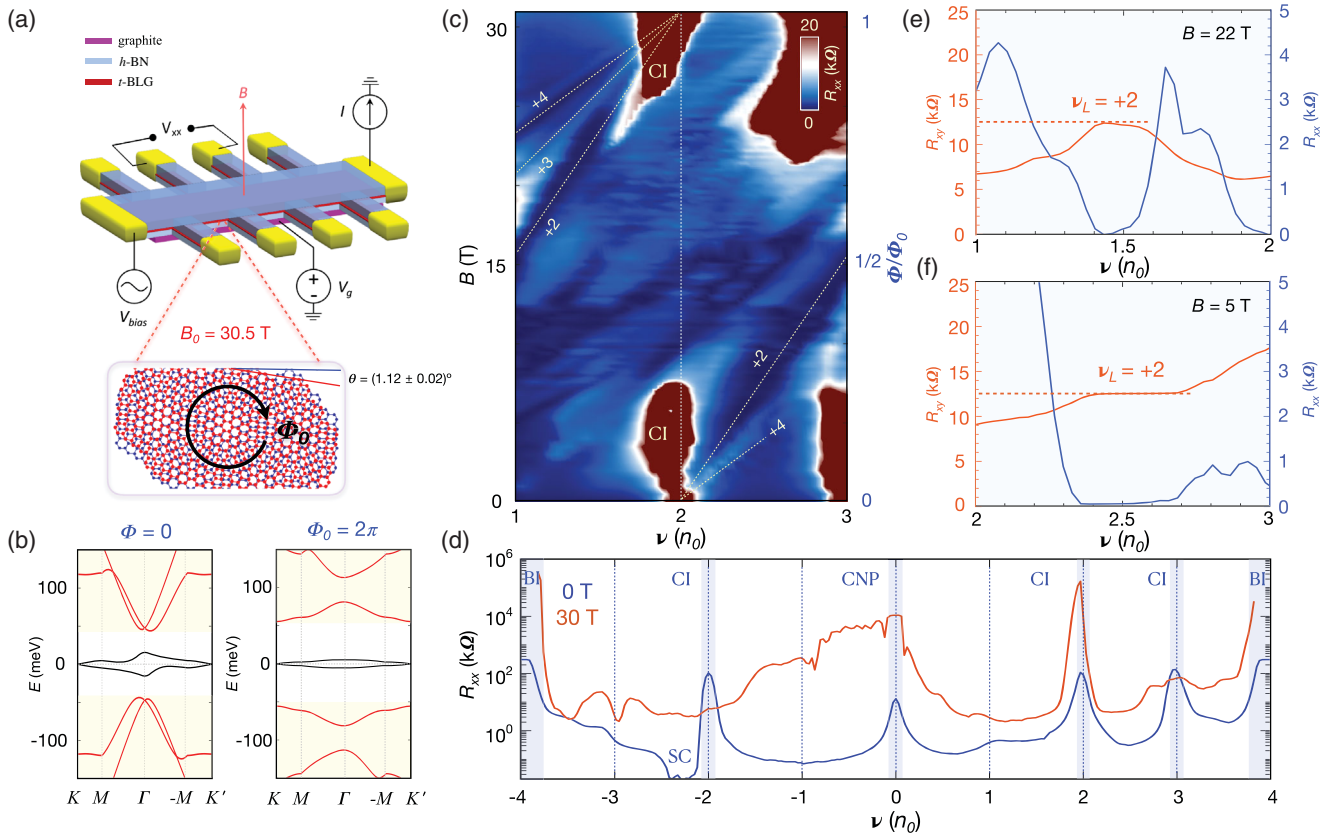

FIG. 1. (a) Schematic of the MATBG device with the performed measurement scheme of the back-gated four-terminal R_{xx} and R_{xy} measurements. The twist angle of the device is $\theta = 1.12° \pm 0.02°$, which results in $B_0 = 30.5$ T. (b) Band structure at zero and Φ_0 magnetic flux. (c) Color plot of R_{xx} as a function of ν and B measured at $T = 40$ mK around $\nu = 2$, showing the reentrant CI and emergence of LLs. (d) R_{xx} vs ν over the entire range of the flat band at $B = 0$ T and $B = 30$ T, clearly showing the reentrant CI at $\nu = +2$ close to Φ_0. (e) and (f) R_{xx} and R_{xy} as a function of ν at $B = 22$ T and $B = 5$ T, respectively, showing full quantization of the $\nu_L = +2$ LL gap.

fillings and interaction-driven Fermi-surface reconstructions, evidenced by new sets of Landau levels originating from these. We also study the higher energy passive bands, where we observe a rich interaction-reconstructed Hofstadter spectrum.

Figure 1(a) shows the schematic of the device, which comprises a van der Waals heterostructure of graphite/h-BN /MATBG/h-BN, where the h-BN layers were specifically nonaligned with the MATBG. We performed four-terminal longitudinal resistance R_{xx} and Hall resistance R_{xy} measurements where the carrier density n of the band is continuously tuned by a gate voltage V_g. The total carrier density n is normalized by $n_S = 4n_0$, where n_S is the density of the fully filled spin and valley degenerate moiré bands and n_0 is the density per flavor. The filling factor of the carriers per moiré unit cell is defined as $\nu = n/n_0$.

Figure 1(b) illustrates the band structure of MATBG with $\theta = 1.12°$ at zero flux and at Φ_0. The zero-flux band structure comprises two connected nearly flat topological bands and higher-energy dispersive bands. An exact study of the BM Hamiltonian in magnetic flux predicts the emergence of a set of low-energy flat bands at Φ_0 but with different symmetry and topology from the zero flux flat bands [17].

Figure 1(d) shows the line plots of R_{xx} vs ν at $B = 0$ T (zero flux) and $B = 30.5$ T (Φ_0) at $T = 40$ mK. The $B = 0$ T trace is dominated by a well-known sequence of resistance peaks [2,3]. The charge neutrality point (CNP) appears to be a gapless phase since R_{xx} is of the order of 10 kΩ. We observe correlated insulators (CI) at $\nu = \pm 2$, $+3$, and band insulators (BI) at $\nu = \pm 4$. In addition, we observe a superconducting region near $\nu = -2$ (see Ref. [28] E). In the $B = 30$ T trace, we observe an overall similar picture, which strikingly shows enhanced resistance peaks at $\nu = +2$ and $+3$: a first indication of reentrant CIs. Temperature dependence of these states (extended data D) shows a clear insulating behavior. Nevertheless, some differences emerge. The CNP is now gapped with a resistance in the order of $R_{xx} \sim 10$ MΩ, and the gaps of the BIs at $\nu = \pm 4$ are enhanced. We also do not find signatures of superconductivity. We argue that the experimental parameters to observe SC are much more stringent than the CIs. Having a low critical magnetic field ($B_c \sim 50$ mT) makes this system very challenging

to observe SC at Φ_0 flux. Since a tiny twist-angle inhomogeneity of $\Delta\theta = 0.05°$ will give rise to a variation of the full flux value by $\Delta B = 60$ mT, which is enough to fully suppress the SC state. We have discussed this in detail in extended data *E*.

To highlight the reentrant behavior of the $\nu = 2$ CI at Φ_0, we show the evolution of the R_{xx} vs v in the B field in the color plot of Fig. 1(c). The ν-B phase space appears to be nearly symmetric about the point corresponding to $\nu = 2$ and $B = 15$ T $= 0.5\ \Phi_0$, under an approximate symmetry sending ν to 4-ν and B to Φ_0-B. At $B = 0$ T we observe a set of Landau levels with LL filling factors $\nu_L = +2, +4$, etc. originating from the CI at $\nu = 2$. The LL with $\nu_L = +2$ was previously interpreted as a correlated Chern insulator (CCI) with a Chern number $C = 2$ [29]. The corresponding R_{xx} and R_{xy} vs ν line traces for $B = 5$ T are plotted in Fig. 1(f), which show clear quantum Hall signatures of $\nu_L = +2$ with $R_{xx} \sim 0\ \Omega$ and $R_{xy} \sim 12.5$ kΩ. The strong interaction opens up a gap at $\nu = 2$ and reconstructs the Fermi surface, which results in a degeneracy of 2 by lifting the fourfold spin-valley degeneracy.

The CI is continuously suppressed with increasing B and vanishes at $B \sim 8$ T, where the phase diagram becomes dominated by LLs. Strikingly, above $B > 24$ T the $\nu = 2$ CI state reappears and grows continuously stronger up to Φ_0 (see Ref. [28] *C*). While due to experimental limitations we could not measure our device in B fields well above Φ_0, by continuity, all the LLs that point away from the CNP above B_0, will point toward the CNP below B_0. Similar to zero flux, we also observe the emergence of a set of LLs from $\nu = 2$ and Φ_0, with $\nu_L = +2, (+3), +4, (+5)$. Here, the even fillings are more pronounced than the odd ones, as can be seen in Fig. 1(e), which shows the quantum Hall traces at $B = 22$ T. In summary, the occurrence of an insulating state which is accompanied by a Fermi-surface reconstruction at Φ_0 firmly establishes the existence of a reentrant $\nu = 2$ CI. Since the most dominant LL here is the $\nu_L = +2$, we also speculate that this LL can be interpreted as a CCI with $C = 2$, in direct analogy to the $B = 0$ T case [29].

We further examine the full ν-B phase space of the flat bands. Figures 2(a) and 2(b) show the respective Landau fan diagrams of R_{xx} and R_{xy} as a function of ν and B, where the observed LLs are schematically laid out in Fig. 2(c). At 0 flux we observe a set of LLs with degeneracy 2 originating from $\nu = \pm 2$, fully nondegenerate LLs from the CNP, LLs with $\nu_L = \pm 3$ from $\nu = \pm 1$, and LLs with $\nu_L = \pm 1$ from $\nu = \pm 3$, in agreement with previous studies [29–32].

At Φ_0, we observe a multitude of new sets of LLs emerging from the different integer fillings ν, demonstrating abundant Fermi-surface reconstructions. Surprisingly, it appears that all the Fermi surfaces have a fully lifted degeneracy, where from $\nu = +1$ we find LLs with the sequence $\nu_L = +1, +2, +3$, from $\nu = \pm 2$ we find LLs with

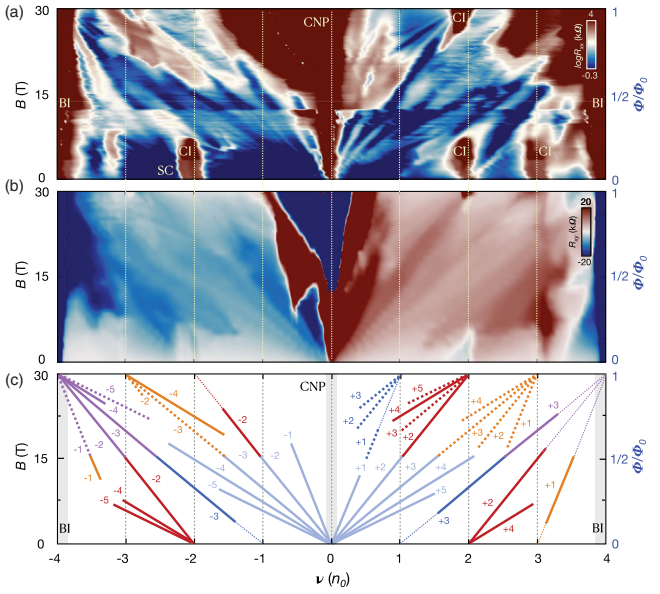

FIG. 2. (a) and (b) show, respectively, the color plots of R_{xx} and R_{xy} as a function of B and v, for the full magnetic phase space from $B = 0$ T to $B = 31$ T and v from −4 to 4. (c) Schematics of all the LLs emerging from different fillings of the band from both zero flux and Φ_0. Light blue lines from the CNP indicate the LLs with $\nu_L = \pm 1, \pm 2, \pm 3, \pm 4$, and ± 5. Dark blue lines indicate the LLs from $\nu = \pm 1$ at both zero flux and Φ_0. Dark red lines correspond to LLs from $v = \pm 2$ at both zero flux and Φ_0. Orange lines indicate the LLs that emerge from $\nu = \pm 3$ and purple lines correspond to LLs from $\nu = -4$. Solid lines mark well-pronounced, quantized LLs, while dashed lines mark much weaker, nonquantized levels.

$\nu_L = \pm 2, \pm 3, \pm 4, \pm 5$, and from $\nu = \pm 3$ we find LLs with $\nu_L = \pm 1, \pm 2, \pm 3$, and ± 4. This suggests that for both odd and even integers the spin and valley degeneracies have been lifted at Φ_0 in contrast to zero flux. This can be attributed to the breaking of $C_{2z}T$ symmetry by magnetic flux [18,33–35] which lifts the degeneracy of the quasiparticles on top of the CIs, although quantitative predictions have not been made so far at odd fillings. Furthermore, we also observe LLs which survive through the full range of magnetic field and connect two different integer fillings at zero flux and at Φ_0. Whereas Ref. [17] uses a strong coupling approach to analyze the ground states at Φ_0, more theoretical work is required to study the interactions within the Hofstadter subbands at intermediate flux.

The strong interaction at zero flux spontaneously breaks the $C_{2z}T$ symmetry and can give rise to several Chern bands at different odd integer fillings [17,33,36]. At Φ_0, the $C_{2z}T$ symmetry is broken by the magnetic field, leading to different single-particle topology in the flat bands and different degeneracies in the many-body charge excitations atop the CI states [17]. The observed differences in the $B = 0$ T and $B = 30.5$ T LLs reflect the importance of symmetry and topology in determining the

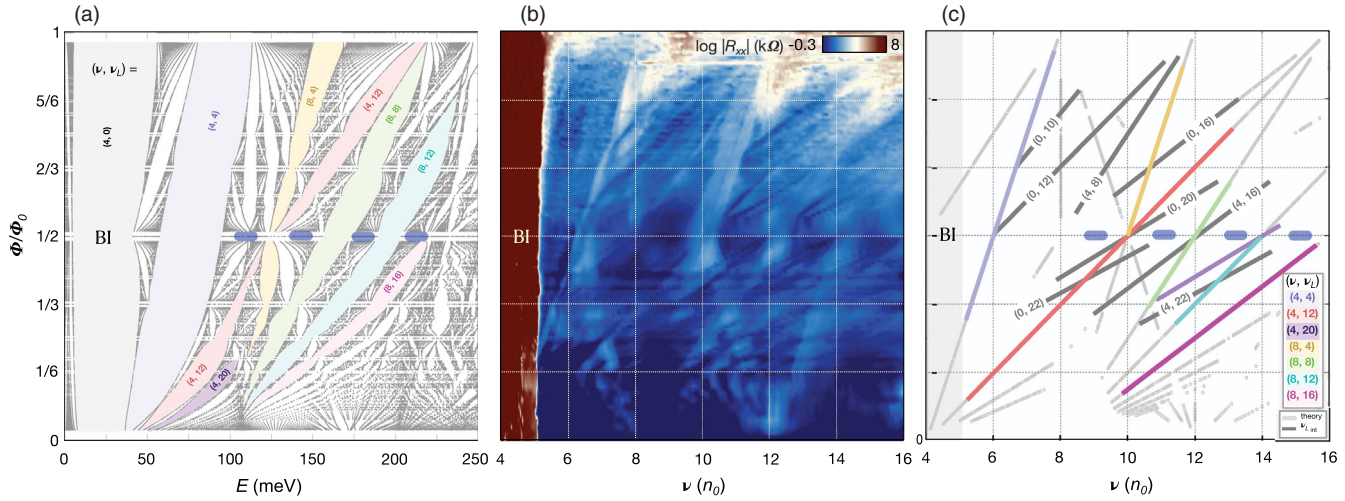

FIG. 3. (a) Calculated Hofstadter spectrum of the BM model for positive energy as a function of the magnetic flux Φ through the moiré unit cell. Different solid gray (4, 0), blue (4, 4), red (4, 12), yellow (8, 4), green (8, 8), cyan (8, 12), magenta (8, 16) and purple (4, 20) regions correspond to the evolution of dominant LL gaps. They are marked with the band filling and filling factor of the LLs (ν, ν_L). (b) Color plot of $\log(R_{xx})$ as a function of B and v for high range of carrier density up to $\nu = 16$. (c) Schematics of (b) and the comparison with (a), where gray circles mark the theoretically predicted gaps from (a) and colored lines mark the strongest LLs in (b). The observed LLs from (b) are plotted with the same color code as the corresponding LLs in (a). Dark gray lines correspond to LLs, which are not predicted from the Hofstadter calculations. These levels are the result of strong interactions in the system (ν_{Lint}). The horizontal blue bars denote metallic regions in (a) matching the high conductance regions (dark blue regions) observed in (b).

many-body phases. The observation of these LLs and the interaction-driven CIs confirms the existence of the (theoretically predicted) flat bands at Φ_0.

The higher energy passive bands in MATBG have larger bandwidth than the flat bands and are amenable to a single-particle Hofstadter analysis. Using the new gauge-invariant formalism of [37], we numerically compute the spectrum to very high accuracy between $\Phi = 0$ and Φ_0. The results are shown in Fig. 3(a) where the Chern numbers of the largest gaps are computed using Wilson loops and the Streda formula. We emphasize that our calculations are exact within the BM model, and do not rely on $\boldsymbol{k} \cdot \boldsymbol{p}$ approximations near the Fermi surfaces. To access this regime experimentally, we have tuned the carrier density above $\nu > 4$. Figure 3(b) shows the color plot of R_{xx} as a function of the normalized magnetic flux and ν. The strongest LLs, observable as lines with slope $1/\nu_L$, are schematically laid out in Fig. 3(c) with corresponding (ν, ν_L), where we find some agreements (but also some disagreements) between the single-particle theory and the observed LLs.

Reference [14] demonstrated that at zero flux, the second through fifth bands of the BM model, counting from CNP, form an elementary band representation and are forced to be connected by symmetry. Hence, no gap is expected in the resistance data [Fig. 3(b)] between $\nu = 4$ and $\nu = 20$ at 0 flux, although there is a Dirac point at $\nu \sim 12$ leading to a low density of states (see Ref. [28] F). This can be seen in Fig. 3(b) from the deep blue conducting regions near $B = 0$, which are punctuated by the less conductive (lighter blue) region near $\nu = 12$. The full-density Bloch bands at zero flux split into Hofstadter subbands upon applying a magnetic flux, giving rise to gaps at fractional fillings. The Chern number C of the gaps is given by the Streda formula: $N = pC\,|q|$, where N is the number of Hofstadter subbands that have been filled, as measured from CNP. At fractional filling ($N \neq 0\ |q|$) C must be nonzero. When interactions, spin-orbit coupling, and the Zeeman effect are neglected, all bands are fourfold degenerate because of the spin and valley degeneracy.

From $\Phi = 0$ to $\Phi \sim 0.5\Phi_0$, there are three prominent features in the Wannier diagram [Fig. 3(c)] appearing at $\nu = 4$, 8, and 12. Near $\nu = 4$, we predict and observe positive slope LLs emerging from the band edge which can be attributed to the low-energy Rashba point in the passive bands of the zero flux BM model [29]. More interesting are the LLs which are connected to $\nu = 8$. Although there is no band edge at $\nu = 8$ in the BM model, the magnetic field breaks the C_{2x} and $C_{2z}T$ symmetries that enforce the second and third bands to be connected. Thus, we can understand the LLs pointing to $\nu = 8$ as indicating a nascent band edge which is revealed by flux in precise agreement with Fig. 3(a), which demonstrates strong gaps originating from $\nu = 8$, with Chern numbers 4, 8, 12, and 16. We expect increased R_{xx} in the regions where LLs of different slopes cross [29]. This is observed in Fig. 3(b) near $\nu = 10$ where the (8, 4) and (12, −4) LLs collide near $0.5\Phi_0$. Additionally, at $0.5\Phi_0$ flux, we observe very clean, highly conducting regions in Fig. 3(b) between the Chern gaps at $\nu = 8$, 10, 12, 14, and 16, corresponding to the

metallic regions in the Hofstadter spectrum (see Ref. [28] *F*), marked by light blue bars in Figs. 3(a) and 3(c).

Some LLs in Figs. 3(b) and 3(c) with $\nu_L = 10$, 18, 22 (not divisible by 4) cannot be explained by the single-particle Hofstadter calculations and rely on interactions to break the spin-valley degeneracy. These LLs originate from the strongly interacting flat bands at zero flux and appear to remain competitive many-body states even at large flux and high fillings. There are also LLs with $\nu_L = 8$, 16 (divisible by 4) and 22 from $\nu = 4$ which do not appear in our single-particle calculations. Further work is necessary to characterize these states.

In summary, we report the first observation of interaction-driven correlated insulating phases at one flux quantum per moiré unit cell in MATBG. Our experimental observations largely agree with our single-particle Hofstadter calculations, which predict the emergence of a set of electronic flat bands at full flux with different symmetry and topology than the zero-field flat bands. These bands are unstable to the creation of correlated states by interactions [17].

D. K. E. acknowledges support from the Ministry of Economy and Competitiveness of Spain through the "Severo Ochoa" programme for Centres of Excellence in R and D (SE5-0522), Fundacio Privada Cellex, Fundacio Privada Mir-Puig, the Generalitat de Catalunya through the CERCA programme, funding from the European Research Council (ERC) under the European Union's Horizon 2020 research and innovation programme (Grant No. 852927). B. A. B.'s work was primarily supported by the DOE Grant No. DE-SC0016239, the Schmidt Fund for Innovative Research, Simons Investigator Grant No. 404513, and the Packard Foundation. Z.-D. S. was supported by ONR No. N00014-20-1-2303, NSF-MRSEC No. DMR-1420541, Gordon and Betty Moore Foundation through Grant No. GBMF8685 toward the Princeton theory program. B. A. B. also acknowledges support from the European Research Council (ERC) under the European Union's Horizon 2020 research and innovation program (Grant Agreement No. 101020833). I. D. acknowledges support from the INphINIT "laCaixa" (ID 100010434) programme (LCF/BQ/DI19/11730030). K. W. and T. T. acknowledge support from the Elemental Strategy Initiative conducted by the MEXT, Japan (Grant No. JPMXP0112101001) and JSPS KAKENHI (Grants No. 19H05790, No. 20H00354, and No. 21H05233).

*dmitri.efetov@icfo.eu

[1] R. Bistritzer and A. H. MacDonald, Moiré bands in twisted double layer graphene, Proc. Natl. Acad. Sci. U.S.A. **108**, 12233 (2011).

[2] Y. Cao, V. Fatemi, A. Demir, S. Fang, S. L. Tomarken, J. Y. Luo, J. D. Sanchez-Yamagishi, K. Watanabe, T. Taniguchi, E. Kaxiras *et al.*, Correlated insulator behaviour at half-filling in magic-angle graphene superlattices, Nature (London) **556**, 80 (2018).

[3] X. Lu, P. Stepanov, W. Yang, M. Xie, M. A. Aamir, I. Das, C. Urgell, K. Watanabe, T. Taniguchi, G. Zhang *et al.*, Superconductors, orbital magnets and correlated states in magic-angle bilayer graphene, Nature (London) **574**, 653 (2019).

[4] U. Zondiner, A. Rozen, D. Rodan-Legrain, Y. Cao, R. Queiroz, T. Taniguchi, K. Watanabe, Y. Oreg, F. von Oppen, A. Stern *et al.*, Cascade of phase transitions and Dirac revivals in magic-angle graphene, Nature (London) **582**, 203 (2020).

[5] D. Wong, K. P. Nuckolls, M. Oh, B. Lian, Y. Xie, S. Jeon, K. Watanabe, T. Taniguchi, B. A. Bernevig, and A. Yazdani, Cascade of electronic transitions in magic-angle twisted bilayer graphene, Nature (London) **582**, 198 (2020).

[6] Y. Cao, V. Fatemi, S. Fang, K. Watanabe, T. Taniguchi, E. Kaxiras, and P. Jarillo-Herrero, Unconventional superconductivity in magic-angle graphene superlattices, Nature (London) **556**, 43 (2018).

[7] M. Yankowitz, S. Chen, H. Polshyn, Y. Zhang, K. Watanabe, T. Taniguchi, D. Graf, A. F. Young, and C. R. Dean, Tuning superconductivity in twisted bilayer graphene, Science **363**, 1059 (2019).

[8] P. Stepanov, I. Das, X. Lu, A. Fahimniya, K. Watanabe, T. Taniguchi, F. H. Koppens, J. Lischner, L. Levitov, and D. K. Efetov, Untying the insulating and superconducting orders in magic-angle graphene, Nature (London) **583**, 375 (2020).

[9] A. L. Sharpe, E. J. Fox, A. W. Barnard, J. Finney, K. Watanabe, T. Taniguchi, M. Kastner, and D. Goldhaber-Gordon, Emergent ferromagnetism near three-quarters filling in twisted bilayer graphene, Science **365**, 605 (2019).

[10] Y. Saito, J. Ge, K. Watanabe, T. Taniguchi, E. Berg, and A. F. Young, Isospin Pomeranchuk effect and the entropy of collective excitations in twisted bilayer graphene, Nature (London) **592**, 220 (2021).

[11] A. Rozen, J. M. Park, U. Zondiner, Y. Cao, D. Rodan-Legrain, T. Taniguchi, K. Watanabe, Y. Oreg, A. Stern, E. Berg *et al.*, Entropic evidence for a Pomeranchuk effect in magic angle graphene, Nature (London) **592**, 214 (2021).

[12] Y. Cao, D. Chowdhury, D. Rodan-Legrain, O. Rubies-Bigorda, K. Watanabe, T. Taniguchi, T. Senthil, and P. Jarillo-Herrero, Strange Metal in Magic-Angle Graphene with Near Planckian Dissipation, Phys. Rev. Lett. **124**, 076801 (2020).

[13] A. Jaoui, I. Das, G. Di Battista, J. Díez-Mérida, X. Lu, K. Watanabe, T. Taniguchi, H. Ishizuka, L. Levitov, and D. K. Efetov, Quantum-critical continuum in magic-angle twisted bilayer graphene, Nat. Phys. (2022).

[14] Z. Song, Z. Wang, W. Shi, G. Li, C. Fang, and B. A. Bernevig, All Magic Angles in Twisted Bilayer Graphene are Topological, Phys. Rev. Lett. **123**, 036401 (2019).

[15] Hoi Chun Po, Liujun Zou, T. Senthil, and Ashvin Vishwanath, Faithful tight-binding models, and fragile topology of magic-angle bilayer graphene, Phys. Rev. B **99**, 195455 (2019).

[16] J. Ahn, S. Park, and B. Yang, Failure of Nielsen-Ninomiya Theorem and Fragile Topology in Two-Dimensional Systems with Space-Time Inversion Symmetry: Application to

Twisted Bilayer Graphene at Magic Angle, Phys. Rev. X **9**, 021013 (2019).

[17] J. Herzog-Arbeitman, A. Chew, and B. Andrei Bernevig, Reentrant correlated insulators in twisted bilayer graphene at 25 T (2π Flux), arXiv:2111.11434.

[18] Jonah Herzog-Arbeitman, Zhi-Da Song, Nicolas Regnault, and B. Andrei Bernevig, Hofstadter Topology: Noncrystalline Topological Materials at High Flux, Phys. Rev. Lett. **125**, 236804 (2020).

[19] J. Zak, Magnetic translation group II. Irreducible representations. Phys. Rev. **134**, A1602 (1964).

[20] K. Nomura and A. H. MacDonald, Quantum Hall Ferromagnetism in Graphene, Phys. Rev. Lett. **96**, 256602 (2006).

[21] C. R. Dean, L. Wang, P. Maher, C. Forsythe, F. Gahari, Y. Gao, J. Katoch, M. Ishigami, P. Moon, M. Koshino, T. Taniguchi, K. Watanabe, K. L. Shepard, J. Hone, and P. Kim, Hofstadter's butterfly and the fractal quantum Hall effect in moiré superlattices, Nature (London) **497**, 598 (2013).

[22] B. Hunt, J. D. Sanchez-Yamagishi, A. F. Young, M. Yankowitz, B. J. LeRoy, K. Watanabe, T. Taniguchi, P. Moon, M. Koshino, P. Jarillo-Herrero, and R. C. Ashoori, Massive Dirac fermions and Hofstadter butterfly in a van der Waals heterostructure, Science **340**, 1427 (2013).

[23] Y. J. Song, A. F. Otte, Y. Kuk, Y. Hu, D. B. Torrance, P. N. First, W. A. de Heer, H. Min, S. Adam, M. D. Stiles, A. H. MacDonald, and J. A. Stroscio, High-resolution tunnelling spectroscopy of a graphene quartet, Nature (London) **467**, 185 (2010).

[24] L. Wang, S. Zihlmann, M. H. Liu, P. Makk, K. Watanabe, T. Taniguchi, A. Baumgartner, and C. Schönenberger, New generation of moiré superlattices in doubly aligned hBN/Graphene/hBN heterostructures, Nano Lett. **19**, 2371 (2019).

[25] J. Finney, A. L. Sharpe, E. J, C. L. Hsueh, D. E. Parker, M. Yankowitz, S. Chen, K. Watanabe, T. Taniguchi, C. R. Dean, A. Vishwanath, M. Kastner, and D. Goldhaber-Gordon, Unusual magnetotransport in twisted bilayer graphene, arXiv:2105.01870.

[26] L. A. Ponomarenko, R. V. Gorbachev, G. L. Yu, D. C. Elias, R. Jalil, A. A. Patel, A. Mishchenko, A. S. Mayorov, C. R. Woods, J. R. Wallbank, M. Mucha-Kruczynski, B. A. Piot, M. Potemski, I. V. Grigorieva, K. S. Novoselov, F. Guinea, V. I. Fal'ko, and A. K. Geim, Cloning of Dirac fermions in graphene superlattices, Nature (London) **497**, 594 (2013).

[27] G. Gumbs, A. Iurov, D. Huang, and L. Zhemchuzhna, Revealing Hofstadter spectrum for graphene in a periodic potential, Phys. Rev. B **89**, 241407(R) (2014).

[28] See Supplemenatal Material at http://link.aps.org/supplemental/10.1103/PhysRevLett.128.217701 for extended data.

[29] I. Das, X. Lu, J. Herzog-Arbeitman, Z. Song, K. Watanabe, T. Taniguchi, B. A. Bernevig, and D. K. Efetov Symmetry-broken Chern insulators and Rashba-like Landau-level crossings in magic-angle bilayer grapheme, Nat. Phys. **17**, 710 (2021).

[30] P. Stepanov, M. Xie, T. Taniguchi, K. Watanabe, X. Lu, A. H. MacDonald, B. A. Bernevig, and D. K. Efetov, Competing Zero-Field Chern Insulators in Superconducting Twisted Bilayer Grapheme, Phys. Rev. Lett. **127**, 197701 (2021).

[31] A. Uri, S. Grover, Y. Cao, J. A. Crosse, K. Bagani, D. Rodan-Legrain, Y. Myasoedov, K. Watanabe, T. Taniguchi, P. Moon, M. Koshino, P. Jarillo-Herrero, and E. Zeldov, Mapping the twist-angle disorder and Landau levels in magic-angle grapheme, Nature (London) **581**, 47 (2020).

[32] K. P. Nuckolls, M. Oh, D. Wong, B. Lian, K. Watanabe, T. Taniguchi, B. A. Bernevig, and A. Yazdani, Strongly correlated Chern insulators in magic-angle twisted bilayer graphene, Nature (London) **588**, 610 (2020).

[33] J. Kang, B. A. Bernevig, and O. Vafek, Cascades Between Light and Heavy Fermions in the Normal State of Magic Angle Twisted Bilayer Graphene, Phys. Rev. Lett. **127**, 266402 (2021).

[34] N. Bultinck, E. Khalaf, S. Liu, S. Chatterjee, A. Vishwanath, and M. P. Zaletel, Ground State and Hidden Symmetry of Magic-Angle Graphene at Even Integer Filling, Phys. Rev. X **10**, 031034 (2020).

[35] B. A. Bernevig, B. Lian, A. Cowsik, F. Xie, N. Regnault, and Z. Song, TBG V: Exact analytic many-body excitations in twisted bilayer graphene Coulomb Hamiltonians: Charge gap, goldstone modes and absence of cooper pairing, Phys. Rev. B **103**, 205415 (2021).

[36] J. Kang and O. Vafek, Strong Coupling Phases of Partially Filled Twisted Bilayer Graphene Narrow Bands, Phys. Rev. Lett. **122**, 246401 (2019).

[37] J. Herzog-Arbeitman, A. Chew, D. K. Efetov, and B. A. Bernevig, Magnetic Bloch theorem and reentrant flat bands in twisted bilayer graphene at 2π flux (to be published).